

Is the Kok effect a respiratory phenomenon? Metabolic insight using ^{13}C labeling in *Helianthus annuus* leaves

Paul P. G. Gauthier¹ , Natalie Saenz², Kevin L. Griffin^{3,4}, Danielle Way^{5,6,7}  and Guillaume Tcherkez^{8,9} 

¹Department of Geosciences, Princeton University, Princeton, NJ 08544, USA; ²Department of Chemistry, Columbia University, 3000 Broadway NYC, New York, NY 10025, USA;

³Department of Ecology, Evolution and Environmental Biology (E3B), Columbia University, 1200 Amsterdam Avenue, New York, NY 10027, USA; ⁴Department of Earth and Environmental Sciences, Lamont Doherty Earth Observatory, Columbia University, 61 Route 9W, Palisades, NY 10964, USA; ⁵Department of Biology, University of Western Ontario, 1151 Richmond Street, London, ON N6A 5B7, Canada; ⁶Environmental and Climate Sciences Department, Brookhaven National Laboratory, Upton, NY 11973, USA; ⁷Nicholas School of the Environment, Duke University, Durham, NC 27710, USA; ⁸Research School of Biology, Joint College of Sciences, Australian National University, Canberra, ACT 2601, Australia; ⁹Seedling Metabolism and Stress, Institut de Recherche en Horticulture et Semences, INRAE Angers, Université d'Angers, 42 rue Georges Morel, Beaucozéz Cedex 49780, France

Summary

Author for correspondence:

Guillaume Tcherkez

Tel: +61 (0)2 6125 0381

Email: guillaume.tcherkez@anu.edu.au

Received: 14 May 2020

Accepted: 11 June 2020

New Phytologist (2020)

doi: 10.1111/nph.16756

Key words: day respiration, isotopic labeling, Kok effect, photosynthesis, quantum yield.

- The Kok effect is a well-known phenomenon in which the quantum yield of photosynthesis changes abruptly at low light. This effect has often been interpreted as a shift in leaf respiratory metabolism and thus used widely to measure day respiration. However, there is still no formal evidence that the Kok effect has a respiratory origin.
- Here, both gas exchange and isotopic labeling were carried out on sunflower leaves, using glucose that was ^{13}C -enriched at specific C-atom positions. Position-specific decarboxylation measurements and NMR analysis of metabolites were used to trace the fate of C-atoms in metabolism.
- Decarboxylation rates were significant at low light (including above the Kok break point) and increased with decreasing irradiance below $100 \mu\text{mol photons m}^{-2} \text{s}^{-1}$. The variation in several metabolite pools such as malate, fumarate or citrate, and flux calculations suggest the involvement of several decarboxylating pathways in the Kok effect, including the malic enzyme.
- Our results show that day respiratory CO_2 evolution plays an important role in the Kok effect. However, the increase in the apparent quantum yield of photosynthesis below the Kok break point is also probably related to malate metabolism, which participates in maintaining photosynthetic linear electron flow.

Introduction

Illuminated leaves not only assimilate CO_2 via photosynthesis but also produce CO_2 due to photorespiration and day respiration (denoted as R_L hereafter). Here, the term day respiration encompasses all nonphotorespiratory CO_2 -producing fluxes in catabolism (mostly pyruvate degradation, the TCA pathway and the oxidative pentose phosphate pathway). While the rate of photorespiration can be computed from Rubisco kinetics and oxygen response curves, fluorescence, or comparisons of O_2 and CO_2 fluxes, day respiration is a small flux that is technically difficult to measure (Tcherkez *et al.*, 2017a,b). A popular technique widely used to estimate day respiration takes advantage of the 'Kok effect'. The Kok effect was discovered decades ago (Kok, 1948, 1949). It is defined by the abrupt change in photosynthetic quantum yield occurring at very low light intensities, comparable to the light-compensation point. At such low light intensities (incident photosynthetically active radiation (iPAR) typically below

$20 \mu\text{mol photons m}^{-2} \text{s}^{-1}$), photosynthesis increases linearly with irradiance and near the light-compensation point ($c.10 \mu\text{mol photons m}^{-2} \text{s}^{-1}$), there is usually an inflection in the response curve, referred to as the Kok effect. The slope of the light response is steeper (and thus the quantum yield is higher) below than above the inflection point (also referred to as the 'break point'). The linear extrapolation of the intercept from the curve above the break point is believed to represent an estimate of R_L (see Kok, 1949, and for recent examples Griffin & Turnbull, 2013; Crous *et al.*, 2017). In mathematical terms, this effect can be simply formulated as follows:

$$A = k \cdot \text{iPAR} - i \cdot R_n \quad \text{Eqn 1}$$

where A is the net CO_2 assimilation rate, k is the apparent quantum yield of photosynthesis, R_n is the respiration rate in darkness and i the inhibition of respiration by light (so that $R_L = i \cdot R_n$). In the Kok effect, there is potentially a change in k and/or i as

light decreases. In the current understanding of the Kok effect based on a change in day respiration, it is assumed that $i < 1$ below the break point and i increases up to 1 above the break point. In fact, the change in quantum yield has been first attributed to the inhibition of mitochondrial respiration by light: below a certain light level (Kok break point), day respiration increases, causing lower assimilation values and thus a larger apparent quantum yield of net photosynthesis. However, its significance remains somewhat controversial, because alternative, nonrespiratory mechanisms have been proposed to explain the Kok effect, such as: a nonlinear response of photorespiration to light (Cornic & Jarvis, 1972; Cornic, 1977); a drastic change in internal CO₂ mole fraction at very low light (proposed by Farquhar & Busch (2017) but dismissed by Buckley *et al.* (2017) and Gong *et al.* (2018)); a combination of both respiratory and internal CO₂ effects (Yin *et al.*, 2020); or an increase in k below the break point, reflecting higher photochemical yield of photosystem II, Φ PSII (for a review, see Tcherkez *et al.*, 2017a).

Understanding the origin of the Kok effect is of prime importance because estimating day respiration using this effect is common practice (including at the ecosystem level to compare the carbon balance of plant functional groups). Using the Kok effect, day respiration has been suggested to vary between species and also under relevant climatic conditions such as elevated CO₂ (Wang *et al.*, 2001; Ayub *et al.*, 2014) or high temperature (Sharp *et al.*, 1984; Kroner & Way, 2016; Way *et al.*, 2019) or drought (Ayub *et al.*, 2011; Crous *et al.*, 2012). Furthermore, the Kok effect has been observed at the ecosystem level using eddy covariance techniques (Bruhn *et al.*, 2011; Wehr *et al.*, 2016; Keenan *et al.*, 2019). Nevertheless, we still do not know with certainty whether the technique based on the Kok effect gives valid estimates of day respiration.

From a metabolic point of view, the Kok effect could, in principle, be due to a change in catabolism, thereby altering the rate of CO₂ production. Monitoring O₂ exchange (with or without photosynthetic inhibitors) has shown that there is no Kok effect on gross O₂ production by photosynthesis while the effect is visible on net O₂ exchange, suggesting that photorespiration or day respiration could be involved (Healey & Myers, 1971). As mentioned above, three major respiratory mechanisms can yield CO₂: pyruvate oxidative decarboxylation catalyzed by pyruvate dehydrogenases (PDHs), the TCA pathway (TCAP) and the oxidative pentose phosphate pathway (OPPP).

Using mass-balance modeling, it has been suggested that the Kok effect comes from insufficient NADPH generation at low light, compensated for by an increased OPPP activity (Buckley & Adams, 2011). Such an effect could take place in the cytosol while chloroplastic OPPP is inhibited (even at very low light) to allow the activity of the Calvin cycle. It should nevertheless be noted that the Kok effect is observed with both CO₂ and O₂ net gas-exchange (Cornic & Jarvis, 1972; Sharp *et al.*, 1984; Gauthier *et al.*, 2018), suggesting that the CO₂/O₂ ratio does not change. This means that possible modifications in catabolism (CO₂ generation) during the Kok effect have to be compensated for by a comparable change in NAD(P)H re-oxidation by O₂. In the case of OPPP, NADPH can be used by anabolism (including

malate synthesis) and it is unlikely to be quantitatively re-oxidized by O₂. Therefore, an increase in OPPP activity alone seems unlikely to explain the Kok effect. Mitochondrial PDH is regulated by phosphorylation and thus a dephosphorylation at low light could easily explain an increase in day respiration during the Kok effect. However, this has not yet been demonstrated experimentally. In addition, PDH phosphorylation decreases with the photosynthesis inhibitor 3-(3,4-dichlorophenyl)-1,1-dimethylurea (DCMU) (Budde & Randall, 1990), but DCMU suppresses the Kok effect (Healey & Myers, 1971). Also, the use of respiratory inhibitors (SHAM, antimycin A) does not change the Kok effect (Peltier & Sarrey, 1988; Padmavathi & Raghavendra, 2001), suggesting that respiration is not directly responsible for the Kok effect. Low oxygen tends to suppress the Kok effect but not high CO₂ (except super high CO₂ $\geq 10\,000\ \mu\text{mol mol}^{-1}$) (Sharp *et al.*, 1984), suggesting that the change in quantum yield is not caused by photorespiration but rather by metabolic mechanisms sensitive to O₂ mole fraction, such as day respiration and/or the Mehler reaction. Monitoring O₂ uptake on isolated chloroplasts has indeed suggested that the Mehler reaction is proportionally higher at very low light (Malkin, 1968). While all of these studies provide separate insights into the origin of the Kok effect, a complete understanding remains elusive.

Taken as a whole, there are arguments both for and against a respiratory origin of the Kok effect, and the metabolic mechanisms involved are not known. Here, isotopic (¹³C) tracing was used to clarify the role played by metabolic reactions producing CO₂ in the Kok effect. Our working hypothesis was that if the break point visible in the *A/i*PAR curve (Kok break point) is associated with abrupt changes in catabolism, it must be reflected in position-specific decarboxylation rates and ¹³C-enrichment in metabolites. We thus followed the position-specific decarboxylation of [¹³C]glucose in sunflower leaves and examined changes in metabolic pathways as a function of irradiance. This study relies on our understanding that PDH, TCAP and OPPP each lead to decarboxylation of C-atoms from characteristic positions in the parent glucose molecule (Fig. 1). We found that [¹³C]glucose decarboxylation progressively increased as irradiance decreased, but this increase in decarboxylation began at irradiances above the Kok break point. Metabolic changes further suggest a considerable enhancement of catabolic enzyme activities (PDH, TCAP) as well as a transient activation of the malic enzyme. While this profile suggests that augmented glucose degradation by catabolism per se cannot explain the Kok effect, it probably reflects a more general phenomenon whereby triose phosphate catabolism leads to decarboxylation and CO₂ release via multiple reactions, and sustains photosynthetic quantum yield.

Materials and Methods

Plant material

Sunflower seeds (*Helianthus annuus* var. Bashful), were planted in Jiffy peat soil pellets soaked with water and grown for 5–6 d in the laboratory under ambient light. Once first leaves appeared, plantlets were transferred to 10-l pots filled with potting mix

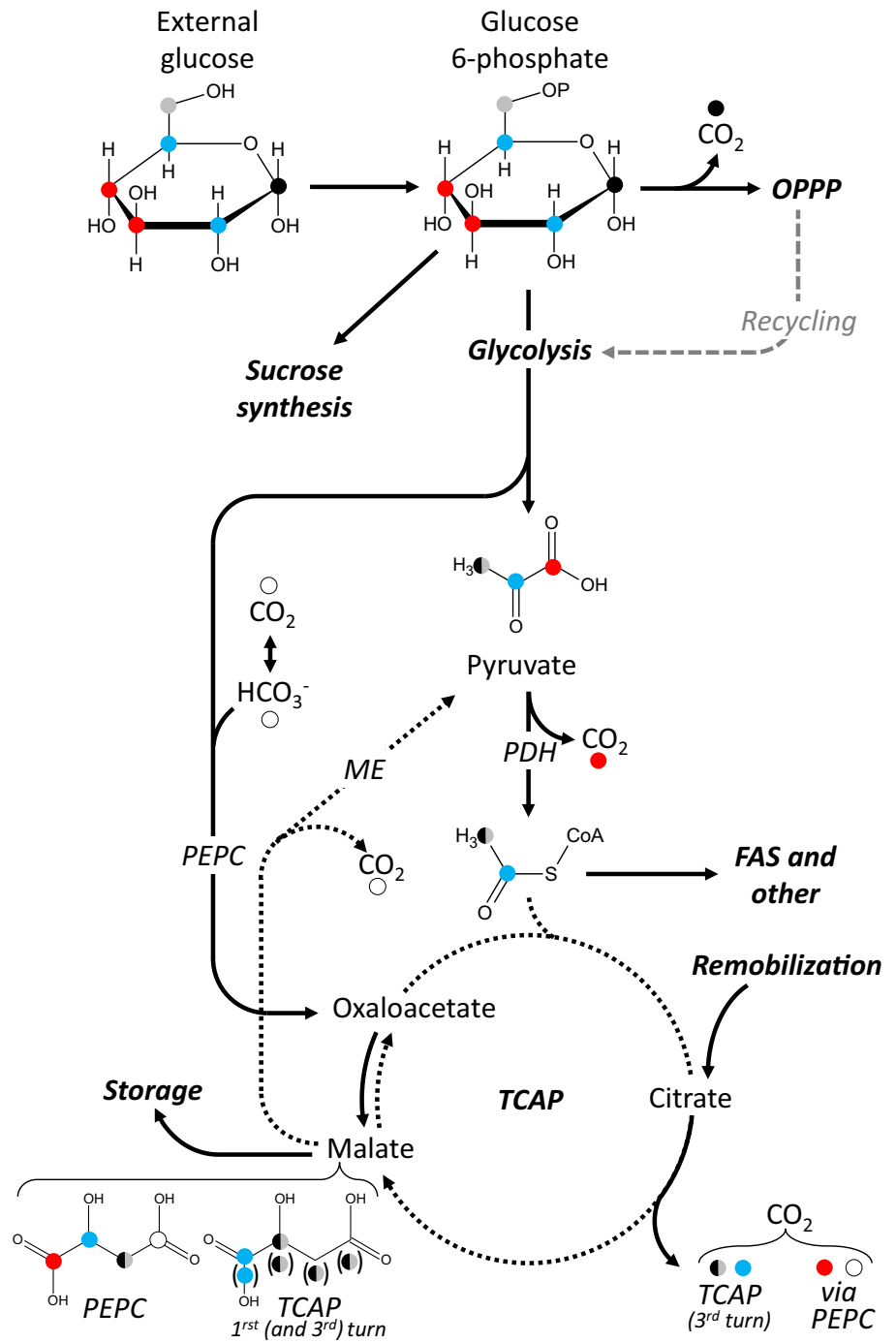


Fig. 1 Scheme representing the fate of carbon atoms from glucose. Most of the glucose molecules form sucrose while a small fraction enter the oxidative pentose phosphate pathway (OPPP, decarboxylating the C-1 atom, black), glycolysis (PDH decarboxylates the C-3 and C-4 atoms, red), and the TCAP that ultimately decarboxylates C-1, C-2, C-5 and C-6 atoms. C-2 and C-5 atoms are labeled in blue, and the C-6 atom is labeled in gray. The anaplerotic PEPC-catalyzed fixation is also shown, so that if PEPC-derived oxaloacetate is decarboxylated by the TCAP, it would produce CO₂ from C-3 and C-4, and from bicarbonate (white). The malic enzyme (ME) liberates the C-4 atom of malate, which comes from bicarbonate via the PEPC and also C-1 if symmetrization occurs via fumarase. To facilitate reading, C-atom symmetrization by fumarase is spelt out here, and C-atoms in malate (originating from either PEPC or TCAP) are shown (bottom left). Steps that are known to be slow (down-regulated) in the light under ordinary gas-exchange conditions are shown with black dotted arrows. The potential recycling of OPPP-derived triose phosphates and fructose 6-phosphate is shown with dashed gray lines. CoA, coenzyme A; FAS, fatty acid synthesis. For simplicity, the figure does not show details of glycolysis such as fructose 6-phosphate phosphorylation and reformation, which is a critically regulated step in the light (see Discussion).

(enriched with Miracle-Gro; The Scotts Company LLC, Marysville, WA, USA) and placed in a glasshouse. Photosynthetic photon flux density was maintained during the 16 h photoperiod above 500 μmol m⁻² s⁻¹ using supplemental lighting (high-pressure sodium lights). Air temperature was maintained at 23°C : 14°C, day : night. All pots were watered for 5–10 min two or three times a day depending on plant size using drip irrigation. Nutrient solution (Miracle-Gro enriched with Fe-EDTA) was applied twice a week. Mature green leaves (*c.* 3–4 wk old) were detached from the plants under water and used for experiments.

Gas-exchange

Position-specific glucose decarboxylation rates, net CO₂ assimilation rates and stomatal conductance were measured. In selected samples, gross O₂ production rate (rate of O₂ production from water splitting) was also measured, and used to compute internal conductance. These properties were measured using the gas-exchange cuvette and associated sensors described previously (Gauthier *et al.*, 2018) and recalled in Supporting Information Notes (S1a). The leaf was first illuminated at moderate light

(iPAR = 600 $\mu\text{mol photons m}^{-2} \text{s}^{-1}$) and once the photosynthetic rate was stable, irradiance was decreased progressively in a stepwise manner. Each transition from one light level to another was progressive and took *c.* 10 min. After photosynthetic stabilization, the decarboxylation rate was measured, and this took 30 min to complete. The leaf was then either sacrificed (snap frozen in liquid nitrogen for NMR analysis) or kept in the chamber to carry out decarboxylation measurements at the next light levels.

Leaf labeling

The leaf was labeled in two ways: using H_2^{18}O for measurement of gross photosynthesis and mesophyll conductance as in Gauthier *et al.* (2018) – this technique takes advantage of on-line isotope ratio MS to measure $^{18}\text{O}_2$ production by photosynthesis, compute the gross photosynthetic rate and therefore the carboxylation-to-oxygenation ratio, which is in turn used to calculate internal conductance; or using 10% or 99% ^{13}C -labeled glucose in positions C-1, C-2 and C-3, C-3,4 or uniformly labelled on the six positions. For each experiment, a fully expanded leaf was detached from a plant and the petiole was immediately immersed in tap water. After 30 min in darkness, the leaf area was reduced to *c.* 100 cm^2 to fit into the chamber. The petiole was placed in the reservoir with 22 ml of ^{18}O -labeled water ($\delta^{18}\text{O} \approx 9000\text{‰}$). Glucose concentration was 15 $\mu\text{mol l}^{-1}$, and no glucose was added in negative control experiments. Two labeling conditions were used: unlabeled glucose (^{13}C natural abundance, 1.1%), or [^{13}C]glucose (10% ^{13}C). After having been placed in the reservoir, the petiole was recut under water to remove any potential embolism. The entire system (leaf + petiole + reservoir) was then sealed inside the chamber. In experiments that used ^{18}O -water, the course of leaf water labeling was followed by measuring water transpired by the leaf using the cavity ring-down spectrometer. The leaf was considered to be fully labeled when the isotope composition of outlet water ($\delta^{18}\text{O}_v$) changed by less than 100‰ h^{-1} (compared to *c.* 2000‰ h^{-1} in the first minutes of ^{18}O -labeling).

Calculations of photosynthesis, respiration and glucose decarboxylation

Day respiration (R_L) was measured with the Kok method (extrapolated intercept of the photosynthetic response curve to light), allowing us to verify that the Kok effect was manifested in our samples. Note that R_L does not enter into the calculation of position-specific glucose decarboxylation rates. The respiration rate in the dark was also measured after keeping leaves in darkness for 20 min. R_L was used to compute mesophyll conductance (g_m) and the CO_2 mole fraction at carboxylation sites (c_c) as in Gauthier *et al.* (2018). [^{13}C]glucose decarboxylation was calculated by mass-balance from the observed difference in the isotope composition of outlet and inlet air, using a method similar to that given previously (Tcherkez *et al.*, 2005, 2008). This calculation yields estimates of apparent decarboxylation, assuming that no respiratory CO_2 is re-assimilated (the issue of refixation is addressed below). The $\delta^{13}\text{C}$ of outlet CO_2 was higher than that

of inlet CO_2 because of decarboxylation of [^{13}C]glucose, as well as the photosynthetic isotope fractionation against $^{13}\text{CO}_2$. The mass-balance of CO_2 fluxes in the leaf cuvette is such that:

$$A = F_{\text{in}} - F_{\text{out}} + F_{\text{Glc}} \quad \text{Eqn 2}$$

where A is net CO_2 assimilation rate, F_{in} and F_{out} are inlet and outlet CO_2 fluxes, respectively, and F_{Glc} is the decarboxylation flux. Note that F_{in} and F_{out} (in $\mu\text{mol m}^{-2} \text{s}^{-1}$) can be written as $c_c \cdot D/S$ and $c_o \cdot D/S$, respectively, where c_c and c_o are inlet and outlet CO_2 mole fractions, and D and S are air flow (mol s^{-1}) and leaf surface area (m^2). In this equation, respiration of unlabeled glucose is included into $F_{\text{in}} - F_{\text{out}}$, that is, the decarboxylation of ^{13}C -glucose is assumed to be an additional, separate flux. Equations for mass-balance of ^{12}C and ^{13}C are as follows:

$$^{12}A = (1 - p_{\text{in}})F_{\text{in}} - (1 - p_{\text{out}})F_{\text{out}} + (1 - p_{\text{Glc}})F_{\text{Glc}} \quad \text{Eqn 3}$$

$$^{13}A = p_{\text{in}}F_{\text{in}} - p_{\text{out}}F_{\text{out}} + p_{\text{Glc}}F_{\text{Glc}} \quad \text{Eqn 4}$$

where p stands for the ^{13}C mole fraction ($= R/(1 + R)$, where R is the $^{13}\text{C}/^{12}\text{C}$ isotope ratio). By definition, the $^{12}\text{C}/^{13}\text{C}$ isotope effect is $\alpha = 1 + \Delta$, where Δ is the observed isotope discrimination associated with net photosynthesis. Therefore, the isotope ratio in net assimilated carbon (R_A) is:

$$R_A = \frac{^{13}A}{^{12}A} = \frac{R_{\text{out}}}{\alpha} \quad \text{Eqn 5}$$

Combining Eqns 3–5 gives the following:

$$F_{\text{Glc}} = \frac{p_{\text{out}}F_{\text{out}}\left(1 - \frac{1}{\alpha}\right) + F_{\text{in}}\left(\left(1 - p_{\text{in}}\right)\frac{1}{\alpha} - p_{\text{in}}\right)}{p_{\text{Glc}} - \left(1 - p_{\text{Glc}}\right)\frac{1}{\alpha} - p_{\text{out}}} \quad \text{Eqn 6}$$

which is identical to Eqn 4 in Tcherkez *et al.* (2005) by neglecting second-order terms and using the delta notation:

$$F_{\text{Glc}} = \frac{\Delta F_{\text{out}} + (\delta_{\text{out}} - \delta_{\text{in}} - \Delta)F_{\text{in}}}{\delta_{\text{Glc}} - \delta_{\text{out}} + \Delta} \quad \text{Eqn 7}$$

Further explanations on how Eqn 6 was implemented, calculations accounting for refixation and calculation of the photosynthetic isotope effect α in Eqn 6 (fractionation Δ in Eqn 7) are provided in Figs S1 and S2 and Notes S1(b–d).

NMR analyses and flux calculations

^1H -NMR analyses of absolute metabolite content were carried out on leaf extracts (10% D_2O) done with 21 mg lyophilized sample in powder extracted with 1 ml phosphate buffer pH 7 (15 mM), using a 700 MHz NMR spectrometer (Bruker Advance III) with water suppression by excitation sculpting. ^{13}C -NMR analyses were carried out on leaf extracts with EDTA (12.5 mM) and maleate (standard; 125 μmol per sample) over 12 500 scans as in Abadie & Tcherkez (2019). Metabolic fluxes were estimated

using a set of differential equations implemented across four steps of 1200 time increments, as in Cui *et al.* (2020). Here, the four steps of interest correspond to the four light transitions (in $\mu\text{mol photons m}^{-2} \text{s}^{-1}$ iPAR): 80-to-60, 60-to-40, 40-to-20 and 20-to-darkness. Metabolic data presented here are mean \pm SD of three replicates, or all three replicates are shown in the figures. Numerical data used as inputs were average values of pool sizes (determined by $^1\text{H-NMR}$) and ^{13}C -enrichments ($\%^{13}\text{C}$; determined by $^{13}\text{C-NMR}$). The contribution of OPPP to triose phosphate generation was calculated from the ^{13}C -enrichment in C-atom positions of sugars (Notes S2). Calculation details and assumptions used to perform computations are detailed in Notes S3.

Results

Photosynthesis response to light

In this study, light response curves of both *A* and the decarboxylation rate of position-specific labeled glucose were measured. Fig. 2 shows net CO_2 assimilation rate as a function of irradiance, with inlet CO_2 kept at the ambient value. As photosynthesis increased, CO_2 around the leaves (c_o) decreased, explaining why photosynthesis tended to saturate at *c.* $10 \mu\text{mol m}^{-2} \text{s}^{-1}$ only at high light. Variations in c_o at low light were very small ($c_o \approx 400 \mu\text{mol mol}^{-1}$) because *A* was close to the compensation point. The Kok effect was clearly visible under our conditions, and linear regressions (continuous lines in Fig. 2) give a break point at $17 \mu\text{mol photons m}^{-2} \text{s}^{-1}$ (Fig. 2, inset), and an extrapolated day respiration rate of $0.48 \mu\text{mol m}^{-2} \text{s}^{-1}$. Average R_d/R_n was 0.44. The quantum yield of photosynthesis (Φ) was *c.* 7% below the Kok break point and 3.6% above, corresponding to a relative change of 50%, consistent with values reported elsewhere (Tcherkez *et al.*, 2017a).

Decarboxylation rates

Position-specific glucose decarboxylation rates (F_{Glc}) were measured at different irradiance and labeling conditions. Fig. 3 shows both absolute (in $\mu\text{mol m}^{-2} \text{s}^{-1}$) and rescaled rates (relative to that at iPAR = $600 \mu\text{mol photons m}^{-2} \text{s}^{-1}$). Position-specific decarboxylation rates in the light were always of the order of $0.01\text{--}0.1 \mu\text{mol m}^{-2} \text{s}^{-1}$, that is, well below the rate of day respiration, simply reflecting the low entry of glucose into catabolism. Note that the average value of the mean decarboxylation rate with nonlabeled glucose was only $0.0002 \pm 0.0001 \mu\text{mol m}^{-2} \text{s}^{-1}$, showing that the system used was associated with a very small uncertainty in measurements themselves. However, there was some variability in F_{Glc} between leaves (even under similar light conditions) because of slight differences in glucose incorporation due to differences in transpiration rate or leaf enzymatic capacities. Therefore, rescaled F_{Glc} values were computed to compare labeling conditions and to reduce variability unrelated to irradiance (for further details on rescaling, see Notes S1b).

There was a very clear increase in decarboxylation rates when irradiance decreased below $100 \mu\text{mol photons m}^{-2} \text{s}^{-1}$, with all

relative F_{Glc} values being larger than 1, that is, larger than the rate observed at $600 \mu\text{mol photons m}^{-2} \text{s}^{-1}$ regardless of the labeled C-atom position. In other words, there was an increase in decarboxylation rates well above the Kok break point (here, $17 \mu\text{mol photons m}^{-2} \text{s}^{-1}$). Despite some variability, there was a tendency for C-3 and C-4 atom positions in glucose to be decarboxylated at a higher rate than C-1 and C-2 atoms (compare black and blue symbols in Fig. 3). When C-atom positions were compared, there was a significant difference ($P < 0.05$ or ≤ 0.07) between C-1/2 and C-3/4, suggesting that a fraction of labeled acetyl-CoA formed by pyruvate dehydrogenase was not decarboxylated. This was also the case in the dark, C-3/4 decarboxylation being *c.* 50% larger than C-1/2 (Fig. 3). It is also worth noting that under our conditions, decarboxylation rates associated with C-1 were indistinguishable from those of C-2 (blue symbols in Fig. 3; see also Fig. S3).

The light-response curve of position-specific decarboxylation rates at low irradiance can be described in two ways. First, when values just above and just below (and at) the Kok break point were compared, there was no significant difference ($P = 0.24\text{--}0.91$), indicating that the Kok break point was not associated with a sudden change in efflux of labeled CO_2 (Table 1). Alternatively, position-specific decarboxylation rates increase by about a factor of 2 between 20 and $0 \mu\text{mol photons m}^{-2} \text{s}^{-1}$. This increase could be attributed to increased respiration rate associated with the Kok effect superimposed upon accelerating decarboxylations associated with diminished light inhibition of glycolysis.

Variations in metabolite content

Samples were also analyzed by $^1\text{H-NMR}$ to quantify metabolic pool sizes (typical spectrum illustrated in Fig. S4). The content in sugars was rather variable but within the same order of magnitude regardless of irradiance, and amino acids such as alanine were always in relatively low abundance (Fig. 4a,b). By contrast, there were considerable changes in the content of metabolites involved in catabolism at low light, in particular an increase in malate from 60 to $40 \mu\text{mol photons m}^{-2} \text{s}^{-1}$ and then a strong decrease from 40 to $20 \mu\text{mol photons m}^{-2} \text{s}^{-1}$ (Fig. 4c), suggesting there was a transient synthesis of malate followed by an abrupt malate degradation. Variations in fumarate content were almost the opposite, showing that malate accumulation took place (at least partly) at the expense of fumarate production. However, citrate showed variations similar to malate, suggesting that changes in malate content were accompanied with citrate production and thus involved the TCAP at some point in metabolism, and not only anaplerosis via phosphoenolpyruvate carboxylase (PEPC). It is also worth noting that other metabolites were present in sunflower leaves, showing the involvement of alternative pathways such as the C_5 -branched pathway (mesaconate) or leucine and valine synthesis (2-oxovalerate, isopropylmaleate) (Figs 4d, S4). In particular, isopropylmaleate was found to accumulate transiently as malate declined at $40 \mu\text{mol photons m}^{-2} \text{s}^{-1}$, suggesting that malate metabolism might have contributed to isopropylmaleate synthesis via

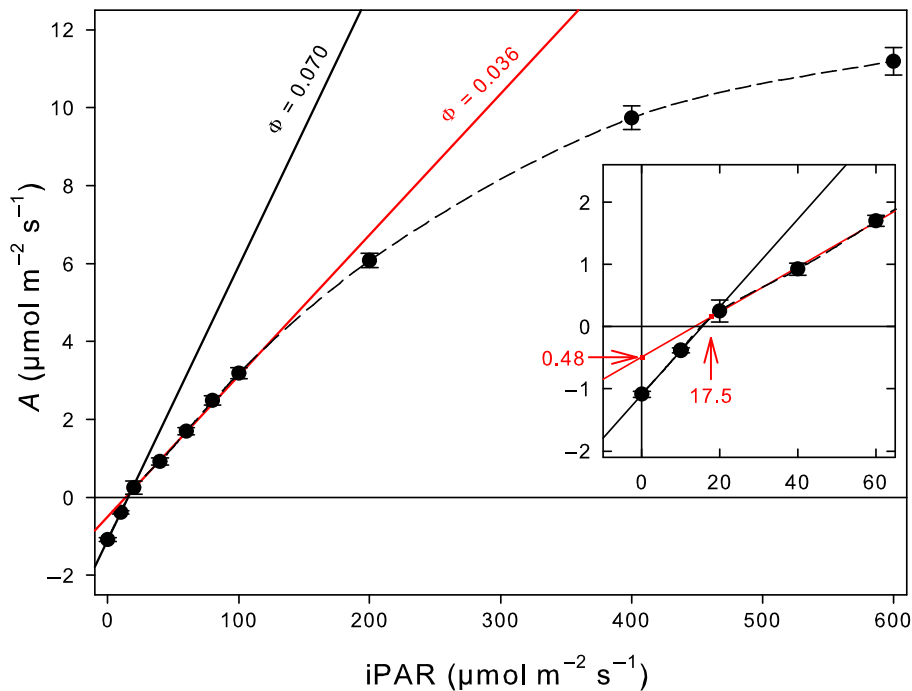


Fig. 2 Light response curve showing the Kok effect at constant inlet CO_2 mole fraction at c. $400 \mu\text{mol mol}^{-1}$, under 21% O_2 in sunflower leaves. Inset, magnification at low light, showing the inflection point at $\text{iPAR} = 17.5 \mu\text{mol photons m}^{-2} \text{s}^{-1}$. The linear extrapolation in red gives the Kok estimate of day respiration (R_l) of $0.48 \mu\text{mol m}^{-2} \text{s}^{-1}$. Each point represents mean \pm SE across all gas exchange experiments ($n = 17$ to 24). The apparent quantum yield of net photosynthesis ($\mu\text{mol CO}_2 \mu\text{mol}^{-1} \text{ photon}$) before and after the inflection point is shown beside regression lines.

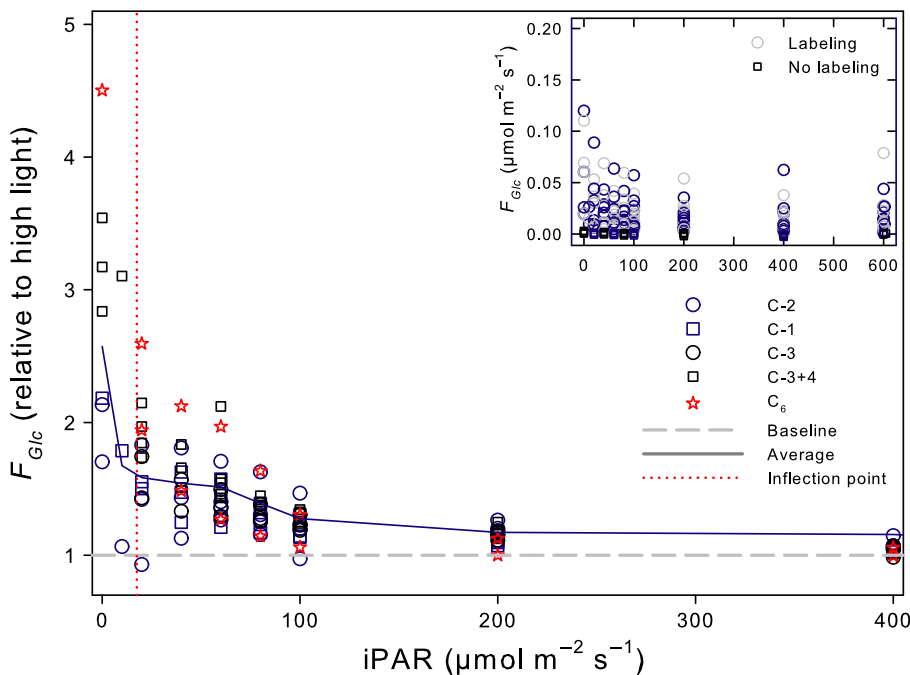


Fig. 3 Glucose decarboxylation rate as a function of irradiance, measured using ^{13}C -enriched glucose (labeled at different C-atom positions) fed to detached sunflower leaves. Main panel: rescaled values (normalized to decarboxylation at high photosynthesis, $600 \mu\text{mol photons m}^{-2} \text{s}^{-1}$ at which $F_{\text{Glc}} = 1$, light-gray dashed line). Different symbols represent the different positional labeling conditions. Inset, absolute (nonrescaled) values directly obtained from Eqn 5, including with no labeling (black open squares). C_6 represents the decarboxylation rate when glucose was totally labeled ($^{13}\text{C}_6$ glucose). The average across all positions is shown with a thick dark-gray line. The light level at which the Kok break point occurs is shown by a vertical red dotted line.

pyruvate regeneration and thus the malic enzyme (also illustrated in Fig. S5).

^{13}C -enrichment in metabolites

Samples associated with ^{13}C -glucose labeling were analyzed by ^{13}C -NMR to look at the ^{13}C redistribution. Isotopic analysis by NMR is only possible for metabolites that are sufficiently concentrated to generate a ^{13}C -signal. That is, minor compounds could not be analyzed. Here, our analysis was thus limited to sugars, malate, citrate, fumarate, succinate, alanine, glutamate and

chlorogenate, the latter being a major secondary metabolite in sunflower (Fig. 5). There was considerable variation in the positional ^{13}C -enrichment with light. In particular, the ^{13}C -enrichment in malate followed the pattern seen in the malate pool size, showing that the increase in malate content at $40 \mu\text{mol photons m}^{-2} \text{s}^{-1}$ and its disappearance at $20 \mu\text{mol photons m}^{-2} \text{s}^{-1}$ were related to de novo synthesis and degradation, respectively. The same was true in citrate, where the ^{13}C -enrichment followed changes in pool size. Succinate and fumarate showed little difference with ^{13}C -natural abundance except at $60 \mu\text{mol photons m}^{-2} \text{s}^{-1}$. This means that whenever fumarate accumulated

Table 1 Average decarboxylation rates of C-atoms in glucose in sunflower leaves at low light.

Irradiance region	C-1 and C-2 atoms		C-3 and C-4 atoms		P-value (positions) Abs./Resc.
	Absolute values ($\mu\text{mol m}^{-2} \text{s}^{-1}$)	Rescaled rate (to high light)	Absolute values ($\mu\text{mol m}^{-2} \text{s}^{-1}$)	Rescaled rate (to high light)	
Just below and at the break point (10–20 $\mu\text{mol m}^{-2} \text{s}^{-1}$)	0.0097 ± 0.0012 (+9%)	1.44 ± 0.13 (+14%)	0.0151 ± 0.0018 (+9%)	1.93 ± 0.36 (+35%)	< 0.03/ 0.07
Just above the break point (40–60 $\mu\text{mol m}^{-2} \text{s}^{-1}$)	0.0089 ± 0.0010	1.42 ± 0.05	0.0138 ± 0.0010	1.43 ± 0.15	< 10 ⁻³ / 0.03
P-value (below vs above)	0.59	0.91	0.53	0.24	

Values shown here are mean ± SE ($n = 7$ to 13) near to and just above the Kok break point ($17.5 \mu\text{mol photons m}^{-2} \text{s}^{-1}$). The P value corresponds to a test (Student–Welsh) made to compare values below ($10\text{--}20 \mu\text{mol photons m}^{-2} \text{s}^{-1}$) and above ($40 \mu\text{mol photons m}^{-2} \text{s}^{-1}$) the break point (bold) and between position types (italics). In parentheses: relative increase below the break point compared to the situation above the break point.

(such as in darkness, Fig. 4), it involved a carbon source weakly labeled by the C-1 atom of glucose, except at $60 \mu\text{mol photons m}^{-2} \text{s}^{-1}$. C-atom positions in glutamate were ^{13}C -labeled but the labeling tended to decline at very low light ($20 \mu\text{mol photons m}^{-2} \text{s}^{-1}$) and in darkness.

These ^{13}C variations seen in metabolites (such as the decrease in $\%^{13}\text{C}$ at very low light) were not due to changes in the isotopic dilution and thus in the ^{13}C -enrichment in glucose, as both glucose and the glucosyl moiety of sucrose showed an increase at very low light and in darkness (Fig. 5d). Parenthetically, the present data show that the maximum $\%^{13}\text{C}$ in metabolite C-atom positions was $c. 5\%$, which matches the maximum enrichment in C-3 of triose phosphates (10% in C-1 of glucose). This shows that in sunflower leaves under our conditions, the metabolically active triose phosphates pool was relatively small and probably labeled maximally in C-3. This is in agreement with the ^{13}C -labeling in C-3/7 in chlorogenate (which comes from C-3 of phosphoenolpyruvate) where, despite some variability, it was strongly labeled at $60 \mu\text{mol photons m}^{-2} \text{s}^{-1}$ (Fig. 5e).

Samples associated with [^{13}C -3] or [$^{13}\text{C}_2$ -3,4]glucose labelling at 60 and $20 \mu\text{mol photons m}^{-2} \text{s}^{-1}$ and in darkness were also analyzed (Fig. 5f). As expected, the ^{13}C -enrichment found in metabolites was much smaller than that observed with [^{13}C -1] glucose labeling, reflecting the fact that ^{13}C atoms were lost as

CO_2 by the PDH (Fig. 1) and thus entered the TCAP to a much lower extent. Still, the $\%^{13}\text{C}$ in succinate C-1/4 occasionally reached $c. 2\%$, suggesting a contribution of the PEPC to feed the TCAP.

Estimation of metabolic fluxes

Pool sizes and $\%^{13}\text{C}$ values were combined into a model based on differential equations to compute metabolic fluxes (described in Notes S3). The comparison of C-atom positions in sugars suggests strongly that the OPPP was associated with a rather small flux, explaining only $c. 7.5\%$ of the total triose phosphate produced by metabolism (Notes S2). The output of calculations is shown in Fig. 6. As expected, most changes in metabolic flux took place during the 40 to $20 \mu\text{mol m}^{-2} \text{s}^{-1}$ transition, that is, when the malate, citrate, fumarate and isopropylmaleate contents changed simultaneously. As a result, the transition to very low light was found to be associated with an increase in PDH, TCAP and PEPC activity (Fig. 6a). The OPPP activity was always very small. There was a transient flux through the malic enzyme, which explained the abrupt decrease in malate from 40 to $20 \mu\text{mol photons m}^{-2} \text{s}^{-1}$. Of course, depending on assumptions made to carry out calculations, there were substantial variations in absolute flux values (Fig. 6a) but the general increase of

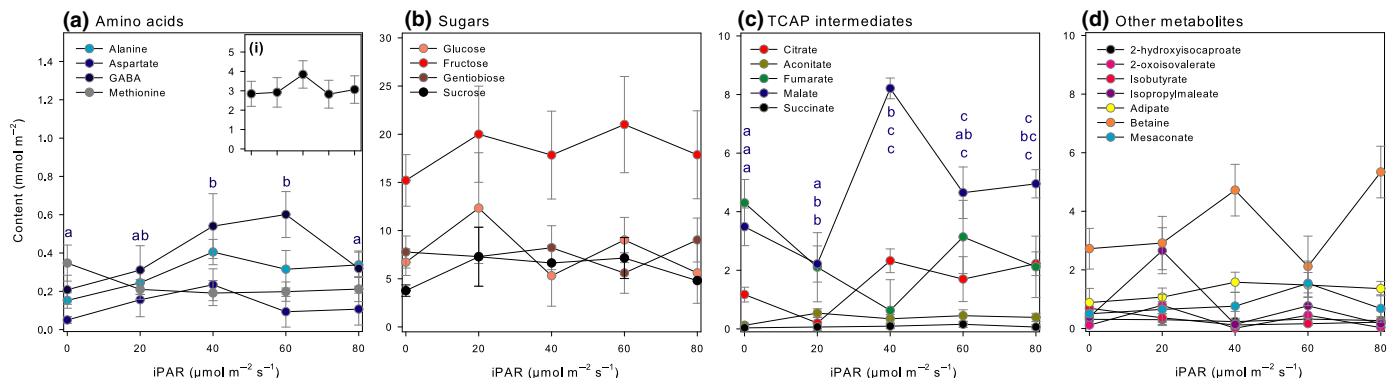


Fig. 4 Metabolic variations in sunflower leaves sampled at low light. Content in metabolites as measured by $^1\text{H-NMR}$: (a) amino acids, (b) sugars, (c) tricarboxylic acid pathway (TCAP) intermediates and (d) other metabolites (including intermediates of the branched amino acid pathway such as isopropylmaleate, in purple). Inset (i) shows the content in amino acids of the glutamate + lysine region (AA in Supporting Information Fig. S4b). In (a) and (c), letters stand for statistical classes ($P < 0.05$) in GABA (a) and malate (blue), fumarate (green) and citrate (red) (b). Note the relatively low content in amino acids (a) compared to organic acids in particular malate or fumarate (c, d). Mean ± SD ($n = 3$).

pathway activities at low light and the transient malic enzyme activity seemed to be robust predictions. When compiled together to predict the CO₂ evolution rate (day respiration), there was a progressive increase in decarboxylation as irradiance declined, from *c.* 1 $\mu\text{mol m}^{-2} \text{s}^{-1}$ to $2 \pm 1 \mu\text{mol m}^{-2} \text{s}^{-1}$ (Fig. 6b). Fluxes could also be used to predict [¹³C-1]glucose decarboxylation rate so as to compare with experimental F_{Glc} values and therefore cross-validate the output of flux calculations. While assumption 1 (supposed low reversibility of fumarase and malate dehydrogenase) was clearly overestimating glucose decarboxylation (continuous line, Fig. 6c), the order of magnitude of predicted rates was in rather good agreement with observed values with the other two assumptions. In other words, flux values that best explained F_{Glc} were between those obtained under assumption 2 (high reversibility and alternative malate utilization) and

assumption 3 (assumption 2 + no steady-state condition for 2-oxoglutarate).

Discussion

Possible causes of the Kok effect are numerous and have been recently reviewed (Tcherkez *et al.*, 2017a). Amongst them, a sudden increase in respiratory decarboxylation as light decreases is the mechanism by which the apparent change in quantum yield was originally explained by Kok (1948). This explains why the Kok effect has been widely used to estimate the rate of day respiration using linear extrapolation. Therefore, our working hypothesis was that the break point visible in the *A/iPAR* curve should be associated with abrupt changes in catabolism. Instead, the results presented here show that metabolic activities do not

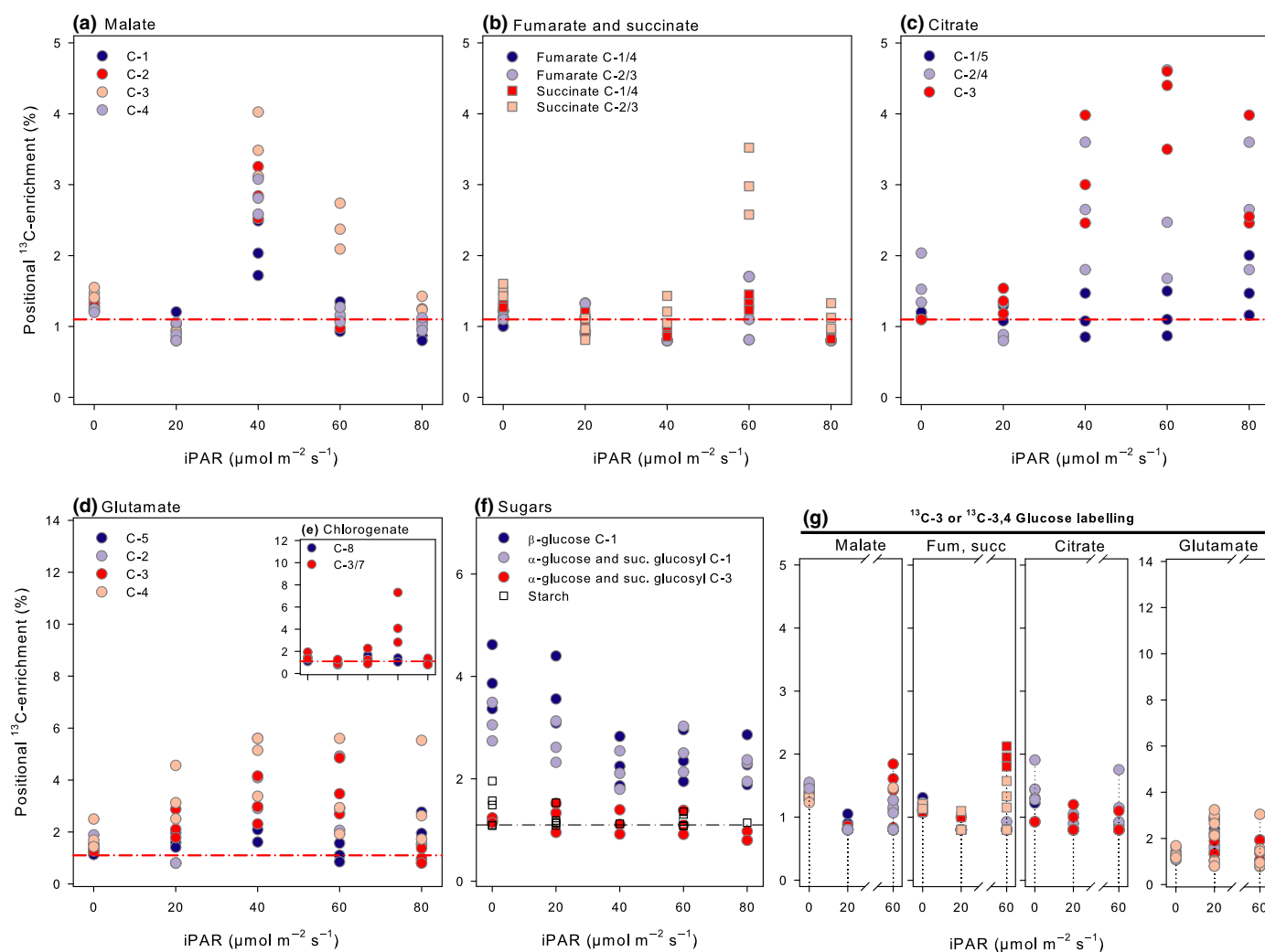


Fig. 5 ¹³C-enrichment pattern in sunflower leaf metabolites upon ¹³C-glucose feeding, with [¹³C-1]glucose (a–f) and [¹³C-3] or [¹³C_{2-3,4}]glucose (g) both at 10% ¹³C (positional enrichment). The ¹³C-enrichment was measured with ¹³C-NMR and is reported in % ¹³C (1.1% representing average natural abundance and this shown with a dashed-dotted red line). For each metabolite, C-atom positions of interest are shown with different symbol colors. In (f), the isotope enrichment in starch (empty squares) was obtained by purification and analysis by isotope ratio MS. Note that starch appeared to be slightly ¹³C-enriched in darkness. Of course, the enrichment of the C-1 atom position in glucose was not equal to 10% due to isotopic dilution by endogenous leaf glucose. Panel (g) shows that contrary to labeling with [¹³C-1]glucose, labeling at C-3 and/or C-4 atom positions leads to minimal enrichment in downstream metabolites, demonstrating the major loss of ¹³C by pyruvate decarboxylation (see Fig. 1). Here, all individual data are displayed to appreciate the variability between samples and how it differentiates from natural abundance.

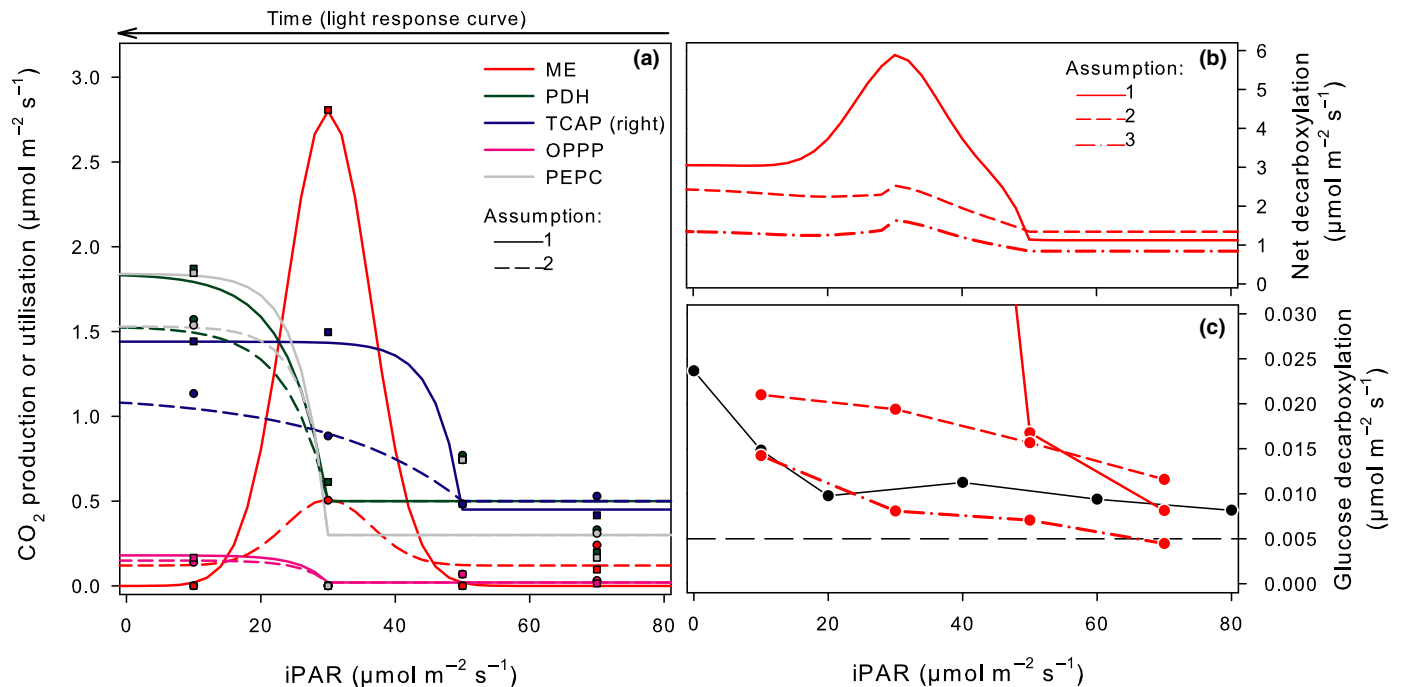


Fig. 6 Estimation of metabolic fluxes at low light, estimated from ^{13}C -enrichment after $[^{13}\text{C}\text{-}1]\text{glucose}$ labeling (Fig. 4) and pool sizes (Fig. 5) in sunflower leaves. (a) Individual flux values obtained for malic enzyme (ME), pyruvate dehydrogenase (PDH), right branch of the Krebs cycle (isocitrate dehydrogenase, 2-oxoglutarate dehydrogenase) (TCAP right), oxidative pentose phosphate pathway (OPPP), and carboxylation by phosphoenolpyruvate carboxylase (PEPC). Two assumptions were used for calculations: low propensity for malate consumption (low reversibility of fumarase and malate dehydrogenase and high malate content: assumption 1, continuous lines and squares), or high propensity for malate consumption (higher reversibility at very low light, minimum change in malate pool size: assumption 2, dashed lines and discs). Under assumption 1, the malic enzyme is responsible for the decrease in malate pool size from 40 to 20 $\mu\text{mol m}^{-2} \text{s}^{-1}$ iPAR. Under assumption 2, this effect is dampened. This panel shows individual values (symbols) and presumed trends to better visualize how fluxes change (lines). (b) Total net decarboxylation summed from (a) under assumption 1 (continuous) and 2 (dashed). Also, a third assumption is presented in which in addition to assumption 2, the TCAP is assumed to account for only one decarboxylation per cycle, a situation that may occur if 2-oxoglutarate is not in the steady-state (dash-dotted). (c) $[^{13}\text{C}\text{-}1]\text{glucose}$ decarboxylation computed with isofluxes obtained from panel (a), using the three same assumptions as in panel (b). The observed (experimental) average values (F_{glc}) are shown in black (from Fig. 2). The dashed horizontal line is the average F_{glc} at high light (200–600 $\mu\text{mol m}^{-2} \text{s}^{-1}$). Note that under assumption 1, the predicted $[^{13}\text{C}\text{-}1]\text{glucose}$ decarboxylation rate is very large (c. 0.1 $\mu\text{mol m}^{-2} \text{s}^{-1}$) at low light and thus beyond the frame of the graph. See also Supporting Information Notes S3 for calculation details.

exhibit an abrupt change at the break point, but rather suggest that the enhancement of respiratory CO_2 evolution is progressive, showing that the increase in day respiration is an important component, but not the sole cause, of the Kok effect.

Catabolic CO_2 production does increase at low light

The results based on $^{13}\text{CO}_2$ evolution from $[^{13}\text{C}]\text{glucose}$ show that there is a clear and significant increase in glucose catabolism when irradiance is low. In fact, $[^{13}\text{C}]\text{glucose}$ degradation to CO_2 progressively increased as light decreased regardless of the ^{13}C -labeled C-atom position (Fig. 3). This pattern was unlikely to be due to a side effect of low light on internal conductance, thereby decreasing refixation. The simplified one-box model calculations predict that accounting for refixation would change absolute rates but not the overall pattern of CO_2 evolution, and there was no relationship at all between position-specific decarboxylation rate and internal conductance (Figs S1, S2). Also, the progressive increase in $^{13}\text{CO}_2$ production as light decreased was also unlikely to be due to isotopic dilution in source triose phosphates, as downstream metabolites could reach maximal $\%^{13}\text{C}$ even at 60 or

80 $\mu\text{mol photons m}^{-2} \text{s}^{-1}$, including chlorogenate C-atoms 3/7, which come from phosphoenolpyruvate (PEP) (Fig. 5e). We note that, by contrast, NMR analysis indicates that the C-1 atom in glucose was between 2 and 4% ^{13}C (Fig. 5f), suggesting an isotopic dilution by the pre-existing glucose pool. NMR analysis of glucose present in leaf extracts reflects total cellular glucose, not the metabolically active pool of glucose 6-phosphate directed to fructose 6-phosphate production. In effect, the corresponding C-atom position in the fructosyl moiety of sucrose appeared to be labeled to a larger extent than its glucosyl moiety (Fig. S6), suggesting that fructose 6-phosphate was indeed turned-over maximally and thus so were triose phosphates. Therefore, our data are consistent with a progressively relaxed inhibition of glycolysis (phosphofruktokinase activity (Stitt, 1990)) and thus glucose degradation and CO_2 production via triose phosphate catabolism.

Respiratory metabolism at low light

$^{13}\text{CO}_2$ decarboxylation was higher when C-3 and C-4 positions were labeled compared to other positions (Table 1). That is, the prevalence of PDH over TCAP decarboxylation is reflected by

the fact that the observed ratio of C-3/4 to C-1/2 decarboxylation rates was larger than unity ($c. 1.6 \pm 0.2$ (mean \pm SE) across all light levels from $iPAR = 10$ to $60 \mu\text{mol photons m}^{-2} \text{s}^{-1}$). This suggests that pyruvate oxidative decarboxylation by PDHs was associated with a larger decarboxylation flux per position than that achieved by the TCAP (or OPPP). At first glance, this may not appear consistent with results obtained previously with French bean, where there was no statistically significant difference in $^{13}\text{CO}_2$ decarboxylation between [^{13}C]glucose labeling in C-1 and C-3 (Tcherkez *et al.*, 2005). This discrepancy comes from the precision of measurements, which is much better here due to higher ^{13}C -enrichment in glucose and thus lower measurement uncertainty ($0.0002 \mu\text{mol m}^{-2} \text{s}^{-1}$ here compared with $0.001 \mu\text{mol m}^{-2} \text{s}^{-1}$ previously). Our present results are broadly consistent with the decarboxylation pattern obtained upon pyruvate feeding of leaves, suggesting larger PDH activity relative to TCAP (reviewed by Tcherkez *et al.*, 2017b). Flux estimates obtained here from $\%^{13}\text{C}$ in metabolites also suggest a larger flux rate via the PDH compared to the TCAP (Fig. 6a). Having said that, the predominance of decarboxylation of glucose C-3 compared to C-1 can be modulated by: the involvement of the malic enzyme, which liberates the C-4 atom of malate which can be labeled after [^{13}C -3]glucose feeding due to equilibration by fumarase (Fig. 1); and the use of stored (nonlabelled) citrate to feed the TCAP and the consumption of TCAP intermediates by N assimilation, which occurs under moderate light (Tcherkez *et al.*, 2009; Gauthier *et al.*, 2010; Abadie *et al.*, 2017). The involvement of the malic enzyme is addressed below. Also, citrate concentrations paralleled those of malate (Fig. 4), suggesting that citrate production depended on malate metabolism – not the opposite. This interdependence of citrate and malate and the possible abstraction of 2-oxoglutarate to feed the synthesis of glutamate were included in flux calculations (Notes S1). Glutamate was visibly labeled (Fig. 5) showing that de novo synthesis of glutamate did not only involve reserves under our experimental conditions.

We further found that CO_2 production by the OPPP was of little importance because C-1 and C-2 labeling led to similar decarboxylation rates (Fig. S3). In addition, direct estimation of OPPP contribution using the scrambling of ^{13}C in sugars indicate that only 7.5% of fructose 6-phosphate molecules originated from the OPPP (Notes S2). For the plants studied here, this result is inconsistent with the hypothesis of Buckley & Adams (2011) that was based on steady-state calculations, in which OPPP was predicted to increase considerably at very low light (and caused the Kok effect) to compensate for the lack of redox power (i.e. NADPH). In addition, on purely biochemical grounds, a lack of redox power is unlikely. In fact, other mechanisms are more likely to meet the potential demand for NADPH at (very) low light, such as the decrease in cyclic electron flux around photosystem I (PSI) and a higher PSII photochemical yield (Oberhuber *et al.*, 1993; Laisk *et al.*, 2005; Kou *et al.*, 2013; Yamori *et al.*, 2016). Mutants affected in cyclic electron flux exhibit a normal electron transport rate and PSI oxidation state at low light (Munekage *et al.*, 2004), and experiments on isolated chloroplasts have suggested that the stromal

NADPH-to-NADP ratio is effectively high at very low light (Heber *et al.*, 1982).

Note that in addition to the general involvement of PDH and TCAP (and the small contribution of OPPP) in decarboxylation across light levels, there were substantial variations in catabolic intermediates (Figs 4, 5) and flux rates (Fig. 6) when light progressively decreased. In particular, there was an enhancement of PDH and TCAP flux rates at very low light, and a transient activity of the malic enzyme. In fact, the peak in malate (both pool size and isotopic enrichment) indicates the probable involvement of enzymes of malate metabolism: malic enzyme and PEPC. Of course, the absolute value of the flux associated with the malic enzyme is rather uncertain, considering changes observed with different calculation assumptions. In particular, oxaloacetate formed by malate oxidation could be used by other pathways (aspartate and lysine synthesis, mesaconate production) and, in addition, mesaconate synthesis leads to $^{13}\text{CO}_2$ production with a metabolic origin (C-4 of oxaloacetate + C-1 of pyruvate) identical to CO_2 evolution by malic enzyme + PDH (Fig. S5). In other words, while the $\%^{13}\text{C}$ and pool size analyses demonstrate important variations in organic acid metabolism, our flux values are just estimates because they could not incorporate alternative metabolic pathways. Also, other metabolites that cannot be easily seen by NMR (in particular C–OH groups that fall in the sugar region) such as tartarate could have contributed to changes in the malate pool.

The transient involvement of the malic enzyme is reminiscent of light-enhanced dark respiration (LEDR), a respiratory transient in darkness where leaf respiration rates are higher after the light has been switched off (for a recent review, see Gessler *et al.*, 2017). In effect, LEDR has been shown to be mostly related to the decarboxylation of malate by the malic enzyme (Gessler *et al.*, 2009), leading to naturally ^{13}C -enriched evolved CO_2 (Barbour *et al.*, 2007). This raises the question of whether the transient increase in malate decarboxylation found here could reflect the beginning of the LEDR phenomenon. In other words, the LEDR observed in the dark might simply be the continuation of malate catabolism started at very low light. Our flux values nevertheless suggest that malic enzyme activity is small during the transition from $20 \mu\text{mol photons m}^{-2} \text{s}^{-1}$ to darkness. At this stage, it is important to remember that the flux values obtained here from samples collected in darkness reflected metabolic events that took place during the transition from $20 \mu\text{mol photons m}^{-2} \text{s}^{-1}$ to darkness plus stabilization in darkness (representing a total of 40 min). Therefore, LEDR was probably finished when the samples were collected, explaining why malic enzyme activity found by flux calculation was small. Further experiments with a much higher time resolution would be required to definitely establish the role of LEDR and the malic enzyme in the Kok effect.

Is the Kok effect caused by day respiration?

A common interpretation of the Kok effect is that day respiration increases when light decreases below the observed break point, and then continues to increase linearly up to night respiration when $iPAR$ equals zero. The results presented here shed light on

metabolic fluxes, but also demonstrate that there are pros and cons for considering a purely respiratory origin of the Kok effect.

On the one hand, it is clear that glucose catabolism increases as irradiance decreases (Fig. 3; see also the section 'Catabolic CO₂ production does increase at low light' above). In addition, at very low light, there is a transient activation of malic enzyme and an enhancement of PDH- and TCAP-catalyzed decarboxylation (Fig. 6a). In other words, there is a progressive increase in day respiration as irradiance drops below 40 $\mu\text{mol photons m}^{-2} \text{s}^{-1}$ (Fig. 6b), which affects net photosynthetic assimilation and thereby increases the apparent slope of the photosynthetic light response curve. In that sense, therefore, respiratory metabolism does participate in the Kok effect.

On the other hand, it seems unlikely that day respiratory CO₂ production is the sole actor responsible for the Kok effect. The increase in glucose decarboxylation rate (either observed (Fig. 3) or reconstituted from calculated fluxes (Fig. 6c)) and thus the up-regulation of catabolism was progressive rather than abrupt (i.e. did not generate a 'break' point), and began significantly above the measured Kok break point. Accordingly, if observed positional decarboxylation rates were used to calculate the potential CO₂ evolution from catabolism of the entire glucose molecule (i.e. $4 \times \text{C-1/2}$ decarboxylation + $2 \times \text{C3/4}$ decarboxylation), the shape of the curve obtained therefrom would not perfectly match what would be expected to explain the Kok effect (Fig. S7a,b). Of course, it can be argued that although the increase in day respiration is nonabrupt, it progresses *linearly*, thereby mimicking a change in quantum yield (while the latter would then remain constant). The predicted shape of day respiration indeed suggests that it could progress sublinearly (calculation assumption 3, Fig. 6). However, when predicted R_L is used in Eqn 1 with a constant quantum yield of 0.036 (found at high light, Fig. 2), the general shape of the curve is relatively close to that of the observed *A/i*PAR curve, but does not perfectly match observed assimilation rates (Fig. S7c) – regardless of the offset of $c. 0.5 \mu\text{mol m}^{-2} \text{s}^{-1}$.

Although the change in CO₂ production itself from respiratory metabolism affects the intercept and the slope (k and i in Eqn 1) insufficiently to explain the Kok break point satisfactorily, this does not mean that the break is unrelated to catabolism. Our metabolic analysis confirms that triose phosphates can be catabolized at very low light (see the Results section). Adenylate and pH monitoring experiments have shown that when stromal NADPH but not ATP is high, typically at low light, triose phosphate production and export from the chloroplast to the cytosol increases (Heber *et al.*, 1982). In this context, glycolysis and the activity of the mitochondrial electron transfer chain could be of importance at low light to: oxidize triose phosphates and maintain linear electron flux in the chloroplast while the Calvin cycle is slow; and favor stromal alkalization and thus ATP synthesis. Here, the chloroplast itself could in principle participate in this process via chloroplastic glycolysis (and pyruvate decarboxylation by chloroplastic PDH) and export of reducing power to the mitochondrion via the malate–oxaloacetate shuttle. The exchange of metabolites between cellular compartments would thus sustain both mitochondrial metabolism and photosynthetic

maintenance. In other words, the Kok effect could be indirectly explained by catabolism via its support to the Calvin cycle. This mechanism contributes to the maintenance of linear electron flux in the chloroplast, and thus tends to increase the quantum yield of photosynthesis (and ΦPSII). This hypothesis was originally formulated by Ulrich Heber in the 1970s (Heber, 1974). A possible scenario would thus be that: just above the 'break point', the stimulation of triose phosphate catabolism leads to an increase in both organic acid pools and the rate of day respiration, with limited impact on maintaining the linear electron flux in the chloroplast; at and below the 'break point', the effect on linear electron flux becomes significant and this makes the Kok effect apparent. For example, the break point could coincide with a critical malate-to-oxaloacetate ratio that allows facile export of redox power from the chloroplast. If true, this scenario would also explain the importance of the transient role of the malic enzyme to regulate the pool of malate at very low light.

Perspectives

To our knowledge, the present study is the first to directly address the metabolic origin of decarboxylated CO₂ in the irradiance region where the Kok effect occurs. It required very challenging experiments with labeling and concurrent measurements of isotope abundance in gases, with a very high precision (because of the very low rates involved). The position-specific decarboxylation rate measurements presented here were done with ¹³C-glucose only, and we recognize that further experiments, with a variety of other substrates (such as citrate, or pyruvate) would provide a more integrative picture of metabolic fluxes along *A/i*PAR response curves. Further work with a higher time-resolution, using high-resolution GC-MS metabolomics (able to distinguish ¹³C₂ and ¹⁸O isotopologues), gas exchange, fluorescence and PSI absorbance monitoring would certainly shed more light on changes in metabolic pools and the origin of the Kok effect, including by monitoring ¹³C-isotope enrichment in quantitatively minor compounds that are not visible by NMR.

Acknowledgements

PPGG was funded by Princeton Environmental Institute Grand Challenge Grant Program. NS acknowledges the support of the Princeton Environmental Institute's Undergraduate Research Fund for senior thesis research at Princeton University. DAW acknowledges the support of the Natural Sciences and Engineering Research Council of Canada and a Visiting Fellow award from the Research School of Biology at ANU. The authors also want to thank Michael Bender for his comments on a previous version of the manuscript and for allowing the utilization of its lab to carry gas exchange measurements. GT thanks the Région Pays de la Loire and Angers Loire Metropole for their funding support through the grant Connect Talent Isoseed. GT also thanks Cyril Abadie for critical reading of the manuscript. The authors acknowledge the support of the NMR facility at the Research School of Chemistry for the isotopic analysis of metabolites, and also thank Hilary Stuart-Williams from the ANU

Isotope Facility for measurements of the isotope composition in starch by EA-IRMS.

Author contributions

PPGG and NS performed gas exchange and labeling experiments to measure decarboxylation rates. GT carried out NMR analyses and metabolic flux calculations, and wrote the first draft of the paper, including figures. PPGG, DW and KLG contributed to the interpretation of the results and participated in finalizing the paper.

ORCID

Paul P. G. Gauthier  <https://orcid.org/0000-0002-2893-7861>
Guillaume Tcherkez  <https://orcid.org/0000-0002-3339-956X>
Danielle Way  <https://orcid.org/0000-0003-4801-5319>

References

- Abadie C, Lothier J, Boex-Fontvieille E, Carroll AJ, Tcherkez G. 2017. Direct assessment of the metabolic origin of carbon atoms in glutamate from illuminated leaves using ^{13}C -NMR. *New Phytologist* 216: 1079–1089.
- Abadie C, Tcherkez G. 2019. In vivo phosphoenolpyruvate carboxylase activity is controlled by CO_2 and O_2 mole fractions and represents a major flux at high photorespiration rates. *New Phytologist* 221: 1843–1852.
- Ayub G, Smith RA, Tissue DT, Atkin OK. 2011. Impacts of drought on leaf respiration in darkness and light in *Eucalyptus saligna* exposed to industrial-age atmospheric CO_2 and growth temperature. *New Phytologist* 190: 1003–1018.
- Ayub G, Zaragoza-Castells J, Griffin KL, Atkin OK. 2014. Leaf respiration in darkness and in the light under pre-industrial, current and elevated atmospheric CO_2 concentrations. *Plant Science* 226: 120–130.
- Barbour MM, McDowell NG, Tcherkez G, Bickford CP, Hanson DT. 2007. A new measurement technique reveals rapid post-illumination changes in the carbon isotope composition of leaf-respired CO_2 . *Plant, Cell & Environment* 30: 469–482.
- Bruhn D, Mikkelsen TN, Herbst M, Kutsch WL, Ball MC, Pilegaard K. 2011. Estimating daytime ecosystem respiration from eddy-flux data. *Biosystems* 103: 309–313.
- Buckley TN, Adams MA. 2011. An analytical model of non-photorespiratory CO_2 release in the light and dark in leaves of C_3 species based on stoichiometric flux balance. *Plant, Cell & Environment* 34: 89–112.
- Buckley TN, Vice H, Adams MA. 2017. The Kok effect in *Vicia faba* L. cannot be explained solely by changes in chloroplastic CO_2 concentration. *New Phytologist* 216: 1064–1071.
- Budde R, Randall D. 1990. Pea leaf mitochondrial pyruvate dehydrogenase complex is inactivated in vivo in a light-dependent manner. *Proceedings of the National Academy of Science, USA* 87: 673–676.
- Cornic G. 1977. *Le dégagement de CO_2 à la lumière chez diverses plantes vertes: étude de la photorespiration et de l'inhibition de la respiration par la lumière*. PhD Thesis, University of Paris-Sud 11 Orsay, France.
- Cornic G, Jarvis PG. 1972. Effect of oxygen on CO_2 exchange and stomatal resistance in Sitka spruce and maize at low irradiances. *Photosynthetica* 6: 225–239.
- Crous KY, O'Sullivan OS, Zaragoza-Castells J, Bloomfield KJ, Negrini ACA, Meir P, Turnbull MH, Griffin KL, Atkin OK. 2017. Nitrogen and phosphorus availabilities interact to modulate leaf trait scaling relationships across six plant functional types in a controlled-environment study. *New Phytologist* 215: 992–1008.
- Crous K, Zaragoza-Castells J, Ellsworth D, Duursma R, Löw M, Tissue D, Atkin O. 2012. Light inhibition of leaf respiration in field-grown *Eucalyptus saligna* in whole-tree chambers under elevated atmospheric CO_2 and summer drought. *Plant, Cell & Environment* 35: 966–981.
- Cui J, Lamade E, Fourel F, Tcherkez G. 2020. $\delta^{15}\text{N}$ values in plants is determined by both nitrate assimilation and circulation. *New Phytologist* 226: 1696–1707.
- Farquhar GD, Busch F. 2017. Changes in the chloroplastic CO_2 concentration explain much of the observed Kok effect: a model. *New Phytologist* 570–584.
- Gauthier PP, Battle MO, Griffin KL, Bender ML. 2018. Measurement of gross photosynthesis, respiration in the light, and mesophyll conductance using H_2^{18}O labeling. *Plant Physiology* 177: 62–74.
- Gauthier PPG, Bligny R, Gout E, Mahé A, Nogués S, Hodges M, Tcherkez GGB. 2010. In folio isotopic tracing demonstrates that nitrogen assimilation into glutamate is mostly independent from current CO_2 assimilation in illuminated leaves of *Brassica napus*. *New Phytologist* 185: 988–999.
- Gessler A, Roy J, Kayler Z, Ferrio JP, Alday JG, Bahn M, Del Castillo J, Devidal S, García-Muñoz S, Landais D. 2017. Night and day-circadian regulation of night-time dark respiration and light-enhanced dark respiration in plant leaves and canopies. *Environmental and Experimental Botany* 137: 14–25.
- Gessler A, Tcherkez G, Karyanto O, Keitel C, Ferrio JP, Ghashghaie J, Kreuzwieser J, Farquhar GD. 2009. On the metabolic origin of the carbon isotope composition of CO_2 evolved from darkened light-acclimated leaves in *Ricinus communis*. *New Phytologist* 181: 374–386.
- Gong XY, Tcherkez G, Wenig J, Schäufele R, Schnyder H. 2018. Determination of leaf respiration in the light: comparison between an isotopic disequilibrium method and the Laisk method. *New Phytologist* 218: 1371–1382.
- Griffin K, Turnbull M. 2013. Light saturated RuBP oxygenation by Rubisco is a robust predictor of light inhibition of respiration in *Triticum aestivum* L. *Plant Biology* 15: 769–775.
- Healey FP, Myers J. 1971. The Kok effect in *Chlamydomonas reinhardtii*. *Plant Physiology* 47: 373–379.
- Heber U. 1974. Metabolite exchange between chloroplasts and cytoplasm. *Annual Review of Plant Physiology* 25: 393–421.
- Heber U, Takahama U, Neimanis S, Shimizu-Takahama M. 1982. Transport as the basis of the Kok effect. Levels of some photosynthetic intermediates and activation of light-regulated enzymes during photosynthesis of chloroplasts and green leaf protoplasts. *Biochimica et Biophysica Acta (BBA) – Bioenergetics* 679: 287–299.
- Keenan TF, Migliavacca M, Papale D, Baldocchi D, Reichstein M, Torn M, Wutzler T. 2019. Widespread inhibition of daytime ecosystem respiration. *Nature Ecology and Evolution* 3: 407–415.
- Kok B. 1948. A critical consideration of the quantum yield of *Chlorella* photosynthesis. *Enzymologia* 13: 1–56.
- Kok B. 1949. On the interrelation of respiration and photosynthesis in green plants. *Biochimica et Biophysica Acta* 3: 625–631.
- Kou J, Takahashi S, Oguchi R, Badger MR, Chow WS. 2013. Quantification of cyclic electron flow in spinach leaf discs. In: Kuang T, Lu C, Zhang L, eds. *Photosynthesis research for food, fuel and future*. Berlin, Germany: Springer, 271–274.
- Kroner Y, Way DA. 2016. Carbon fluxes acclimate more strongly to elevated growth temperatures than to elevated CO_2 concentrations in a northern conifer. *Global Change Biology* 22: 2913–2928.
- Laisk A, Eichelmann H, Oja V, Peterson RB. 2005. Control of cytochrome b6f at low and high light intensity and cyclic electron transport in leaves. *Biochimica et Biophysica Acta (BBA) – Bioenergetics* 1708: 79–90.
- Malkin S. 1968. Analysis of the 'weak light effect' on the fluorescence yield in isolated chloroplasts. *Biochimica et Biophysica Acta (BBA) – Bioenergetics* 153: 188–196.
- Munekage Y, Hashimoto M, Miyake C, Tomizawa K-I, Endo T, Tasaka M, Shikanai T. 2004. Cyclic electron flow around photosystem I is essential for photosynthesis. *Nature* 429: 579–582.
- Oberhuber W, Dai Z-Y, Edwards GE. 1993. Light dependence of quantum yields of Photosystem II and CO_2 fixation in C_3 and C_4 plants. *Photosynthesis Research* 35: 265–274.
- Padmavathi L, Raghavendra AS. 2001. Importance of the cytochrome pathway of mitochondrial electron transport over the alternative pathway during the

- Kok effect in leaf discs of pea (*Pisum sativum*). *Physiologia Plantarum* 113: 430–434.
- Peltier G, Sarrey F. 1988. The Kok effect and the light-inhibition of chlororespiration in *Chlamydomonas reinhardtii*. *FEBS Letters* 228: 259–262.
- Sharp RE, Matthews MA, Boyer JS. 1984. Kok effect and the quantum yield of photosynthesis: light partially inhibits dark respiration. *Plant Physiology* 75: 95–101.
- Stitt M. 1990. Fructose-2,6-bisphosphate as a regulatory molecule in plants. *Annual Review of Plant Physiology and Plant Molecular Biology* 41: 153–185.
- Tcherkez G, Bligny R, Gout E, Mahé A, Hodges M, Cornic G. 2008. Respiratory metabolism of illuminated leaves depends on CO₂ and O₂ conditions. *Proceedings of the National Academy of Sciences, USA* 105: 797–802.
- Tcherkez G, Cornic G, Bligny R, Gout E, Ghashghaie J. 2005. *In vivo* respiratory metabolism of illuminated leaves. *Plant Physiology* 138: 1596–1606.
- Tcherkez G, Gauthier P, Buckley TN, Busch FA, Barbour MM, Bruhn D, Heskell MA, Gong XY, Crous K, Griffin KL *et al.* 2017a. Tracking the origins of the Kok effect, 70 years after its discovery. *New Phytologist* 214: 506–510.
- Tcherkez G, Gauthier P, Buckley TN, Busch FA, Barbour MM, Bruhn D, Heskell MA, Gong XY, Crous KY, Griffin K *et al.* 2017b. Leaf day respiration: low CO₂ flux but high significance for metabolism and carbon balance. *New Phytologist* 216: 986–1001.
- Tcherkez G, Mahé A, Gauthier P, Mauve C, Gout E, Bligny R, Cornic G, Hodges M. 2009. In folio respiratory fluxomics revealed by ¹³C isotopic labeling and H/D isotope effects highlight the noncyclic nature of the tricarboxylic acid “cycle” in illuminated leaves. *Plant Physiology* 151: 620–630.
- Wang X, Lewis JD, Tissue DT, Seemann JR, Griffin KL. 2001. Effects of elevated atmospheric CO₂ concentration on leaf dark respiration of *Xanthium strumarium* in light and in darkness. *Proceedings of the National Academy of Sciences, USA* 98: 2479–2484.
- Way DA, Aspinwall MJ, Drake JE, Crous KY, Company CE, Ghannoum O, Tissue DT, Tjoelker MG. 2019. Responses of respiration in the light to warming in field-grown trees: a comparison of the thermal sensitivity of the Kok and Laisk methods. *New Phytologist* 222: 132–143.
- Wehr R, Munger JW, McManus JB, Nelson DD, Zahniser MS, Davidson EA, Wofsy SC, Saleska SR. 2016. Seasonality of temperate forest photosynthesis and daytime respiration. *Nature* 534: 680–683.
- Yamori W, Kondo E, Sugiura D, Terashima I, Suzuki Y, Makino A. 2016. Enhanced leaf photosynthesis as a target to increase grain yield: insights from transgenic rice lines with variable Rieske FeS protein content in the cytochrome b6/f complex. *Plant, Cell & Environment* 39: 80–87.
- Yin X, Niu Y, Van der Putten PEL, Struik PC. 2020. The Kok effect revisited. *New Phytologist*. doi:10.1111/nph.16638.

Supporting Information

Additional Supporting Information may be found online in the Supporting Information section at the end of the article.

Fig. S1 Relationship between refixation-corrected and uncorrected glucose decarboxylation rate.

Fig. S2 Relationship (or lack thereof) between decarboxylation rates and internal conductance.

Fig. S3 Ratios of decarboxylation rates.

Fig. S4 Example of ¹H-NMR spectrum used to quantify metabolites.

Fig. S5 Potential roles of alternative metabolic pathways.

Fig. S6 Positional ¹³C-enrichment in sugars.

Fig. S7 Relative decarboxylation rates for curve shape comparison.

Notes S1 Gas exchange system and calculations.

Notes S2 Calculation of the contribution of the OPPP.

Notes S3 Metabolic flux calculations.

Please note: Wiley Blackwell are not responsible for the content or functionality of any Supporting Information supplied by the authors. Any queries (other than missing material) should be directed to the *New Phytologist* Central Office.